

A Slit Scanning Depth of Route Panorama from Stationary Blur

Min Shi Jiang Yu Zheng

*Department of Computer Science
Indiana University Purdue University Indianapolis
E-mail: mshi,jzheng@cs.iupui.edu*

Abstract

This work achieves an efficient acquisition of scenes and their depths along streets. During the movement of a vehicle, a slit in the camera frame is set properly to sample scenes continuously for a route panorama. This paper proposes a novel method of depth estimation by analyzing a new phenomenon named stationary blur in the route panorama. We find its relation with the depth and evaluate its degree at local and global levels. The depth estimation through filtering avoids feature matching and tracking that are error-prone in the scanning of real and complex street scenes. Our method provides reliable results but requires much less data than that of the structure from motion. This keeps the elegance of the route panorama in data representation, and is suitable for real time sensor development. Utilizing the completeness of the route panorama in the scene archiving, we can generate planar models of streets, which will be used in city visualization.

1. Introduction

Recently, there are increasing demands for fast construction of urban models for city visualization. Although air-borne laser systems have produced elevation maps, the rendered images viewed from the ground have inadequate resolution, even with the finest LIDAR data. On the contrary, the route panorama (RP) has been proposed for archiving scenes along streets [5,6,7,12].

Continuous views are obtained from the slit scanning as a camera mounted on a vehicle moves along streets. The small data size and seamless scene coverage make the route panorama extendable to a long distance, which is a practical solution of virtual city indexing and navigation via network [5]. The drawback of the route panorama is the deformation of the 2D parallel-perspective projection. This can be overcome by the depth extraction and 3D model rendering.

Targeting a large urban area is more challenging than working in an indoor environment. Because of the large scale of scenes, a stable and efficient approach for sustainable systems has to be explored. Many analysis methods on translating videos have estimated depth of scenes based on the structure from motion using optical flow [15], feature matching [4,16], and EPI tracking [11,12]. Besides the complexity issue of these methods, the entire video volume or image sequence are stored and processed, which makes the real time processing difficult. On the other hand, various laser range finders have been developed for scanning buildings. The shortcoming is the long measuring times at a local position. The most successful system for route scanning is a vehicle-borne laser system [14] that measures depth during movement.

In this work, we propose a unique method to measure the depth from a street. We analyze a new phenomenon named *stationary blur* in the route panorama and find the depth from the degree of the blur. The depth is estimated from the temporal contrast in the RP and the original spatial contrast at the slit. More precise than the motion analysis based on abstract lines of sight, the sampling



Fig. 1 A section of 2D route panorama generated from a slit with its tilt slightly facing up.

process is analyzed. We propose an algorithm that generates more accurate depth but uses much less data than the structure from motion. The stored compact data for depth along with the continuous RP facilitates the post model construction along long routes. We generate planar model of streets for fast VR environment construction.

Related works for 3D scenes require feature matching on two GPVs [1] or image patches [4] scanned in different directions from the path, which are influenced by repetitive patterns on buildings, and frequent occlusions from close range objects. Another problem of these methods is the inconsistent coverage at distance scenes. Although two close viewing directions can diminish the difficulty in matching, the resulting depth of urban scenes has inadequate resolutions. An alternative depth estimation method is to track EPIs in a video volume during the camera translation [11,12,13]. However, it was used at local positions or for short distances. On a real road, EPIs are easily destroyed by unstable camera motion or curved paths. Robust tracking in EPIs is hard to expect. Overall, these approaches have not extended to a long distance.

The difference of this work from others is in determining the depth instantly from local data, according to the *stationary blur*. We evaluate the blur to avoid the feature matching or tracking. A filtering process makes the scanning suitable for real time processing, robust to outdoor motion, and extendable to long distances. Rather than elongating time for more observations, we generate depth directly as the slit scans across a scene. Such a strategy reduces the influences from the varied motion, vehicle shaking, and occlusion in urban environments. It keeps the advantages of the route panorama and will benefit sensor development. The motion is obtained from other reliable sources such as GPS or vehicle control. The model can be constructed by using the obtained depth and motion information at a global level.

As a base, we provide a general model of scanning in Sec. 2, which covers slit setting, shape and motion aspects of the route panorama based on abstract lines of sight. *Stationary blur* is explored at a detailed sampling level in Sec. 3. Local and global estimations of the depth from the stationary blur are in Sec. 4, and experiment in Sec. 5.

2. Acquisition of Route Panoramas

2.1 Camera Motion and Slit Scanning

We define a slit-scanning model that is more general than what has been proposed in [6]. A camera is mounted on a vehicle with its axis perpendicular to the vehicle translation V . The vehicle path is a smooth curve on a horizontal plane, with small disturbances over bumpy roads. A four-wheeled vehicle can realize this motion. We

denote the camera path by $S(t)$ in a global coordinate system, where t is the time of scanning. Such a path is the envelope of circular segments with changing curvature κ . If the vehicle moves along a straight lane, the camera path has curvature $\kappa=0$. The vehicle keeps a speed as constant as possible. The variation in speed and path can be

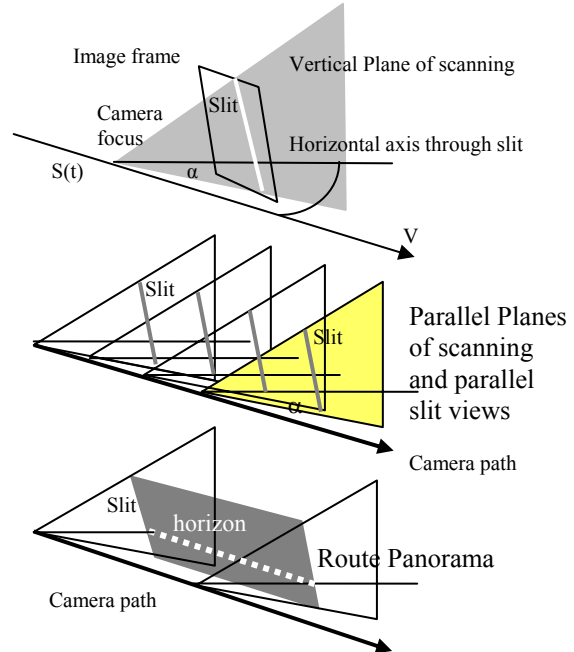


Fig. 2 Camera moves along a path on a horizontal plane.

normalized by reading precise output from GPS as in [8].

In order to produce good shapes in the route panoramas, a plane of scanning (PoS) is set vertical in the 3D space as the camera moves forward (Fig.2). This ensures that vertical lines in the 3D space appear vertically in the RPs even if the camera moves on a curved path. The curves or lines parallel to the camera path are horizontal in the route panorama. The angle α between the PoS and motion vector V determines the viewing aspects of streets, e.g., side view, fore-side view, or rear-side view along the street.

The camera frame intersects with the PoS to form a slit l . The slit may not be vertical in the frame if the camera is tilted up for high buildings (Fig. 3). We calibrate the slit by using a sample image taken when the vehicle is on a horizontal plane. A building with vertical structure lines exists in the image. The vanishing point of the vertical lines is estimated and the slit is programmed to pass the vanishing point for the vertical PoS . From the vanishing point, we calculate the camera tilt, and then the projection of the horizon h in the image. Because of the defined camera direction, optical flow caused by motion V is horizontal for the local translation. For most curved paths

with low curvatures, the flow direction on the slit can still be approximated as horizontal.

We continuously collect the temporal data on the slit (one pixel line) and paste them to another image memory consecutively. The generated route panorama has time t (frame) as its horizontal coordinate and slit y as its vertical coordinate. A fixed sampling rate, normally selected as the maximum reachable frame rate, is used for scanning. The generate route panorama, which has non-redundant scene coverage, is only a slice in the entire video volume. Concurrent to the acquisition of the route panorama, we compute the spatial differential across the slit (involving ± 2 pixels) for later use.

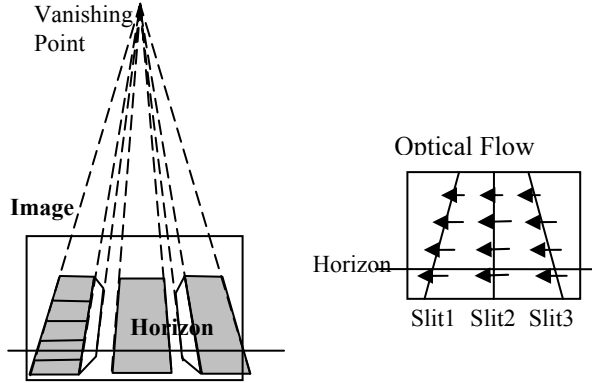


Fig. 3 Example of the programmable slits in the image frame determined from the vanishing point of vertical lines.

The slit scanning approach obtains a 2D route panorama directly. It processes less data than the image stitching because no scene overlapping and inter-frame matching are necessary in the scanning. Mosaicing for a translating camera is not as simple as for a rotating camera. Because the translation yields inconsistent motion parallax at different depths, a perfect 2D image overlapping is impossible. Deforming scenes to a dominant depth yields an irregular scale in the image length; the horizontal coordinate is no longer equal-distance but depth-dependent. The real integration of patches has to be done in 3D space, or equivalently piece-wised image deformation [4]. The mosaicing requires image matching, motion estimation, and intermediate view interpolation, which may be influenced by occlusion and lack of features. If these are not applied at the sensor level, the cost to store the increasing images during the vehicle motion is huge.

2.2 Shape Properties of Route Panoramas

From the projection point of view, scenes at consecutive time instances are projected along the fixed PoS towards the camera path. A parallel-perspective projection is obtained from linear camera motion, and a bended-parallel-perspective projection from curved path. As

depicted in Fig. 2, scenes scanned by one PoS are projected onto the slit view in perspective projection, and entire scenes are projected towards the camera path through the parallel planes of scanning with the same angle α from V . By transforming data on a slit l to the slit l' vertical in the PoS, we can convert a general route panorama to the basic route panorama that is vertical along the camera path. Defining the local camera coordinate system $O\text{-}XYZ$, which has the X axis aligned with V , and vertical Y axis, a 3D point $P(X,Y,Z)$ under the normal perspective projection has the image position (x,y) as

$$I(x,y,t) : x = Xf/Z, y = Yf/Z \quad (1)$$

where f is the calibrated camera focal length. The projection of P in the route panorama through the parallel-perspective projection is $I(t,y) = I(x,y,t)|_{x \in l}$

$$I(t,y) : t = S/r, y = Yf/Z, r = V/m \quad (2)$$

where $V=|V|$, $S=|S|$, m (frame/sec) is the camera frame rate, and r (meter/frame) is the slit sampling interval on the path.

The parallel-perspective projection is different from either perspective projection or parallel projection. Under perspective projection, both horizontal and vertical scales of an object are relative to the depth. While in parallel projection, both scales are absolute. Under parallel-perspective projection, the horizontal scale is absolute while the vertical scale is relative to the depth. Therefore, objects in the route panorama have shape characteristics briefly as follows:

- (1) A distant object looks “wider” in a route panorama than in a perspective image, and looks “lower” than in a parallel projection image.
- (2) Due to the parallel PoS piled horizontally, a 3D line stretching in depth is projected as a hyperbola approaching to a horizontal asymptotic line; such a line in a perspective image is generally slanted and extends to a vanishing point.
- (3) Under bended-parallel-perspective projection of scenes towards a general curved path, 3D lines will be projected as lines or envelopes of hyperbolas in the route panoramas.

2.3 Motion Characteristics at Sampling Slit

Assume point $P(X,Y,Z)$ has translation $V(V,0,0)$ and rotation $\Omega(0,\beta,0)$, where rotation velocity β is a piece-wised constant along a path readable from GPS. The relative velocity of the point to the camera is

$$\frac{\partial P(t)}{\partial t} = -V + \Omega \times P(t) \quad (3)$$

When the point is viewed through the slit at time t , the above can be decomposed to

$$\frac{\partial X(t)}{\partial t} = -V + \beta Z(t) \quad \frac{\partial Y(t)}{\partial t} = 0 \quad \frac{\partial Z(t)}{\partial t} = -\beta X(t) \quad (4)$$

Taking derivative of (1), the image velocity v at the slit

position is

$$v = \frac{\partial x}{\partial t} = f \frac{\partial X / \partial t}{Z(t)} - fX \frac{\partial Z(t) / \partial t}{Z^2(t)} = f \frac{\partial X / \partial t}{Z(t)} - x \frac{\partial Z(t) / \partial t}{Z(t)} \quad (5)$$

For the linear motion, $\beta=0$ so that

$$Z(t) = -f \frac{V}{v} = -fV \frac{\partial t}{\partial x} \quad (6)$$

which is a traditional approach to obtain depth. In order to obtain good estimation of v , feature matching, EPI tracking and Kalman filtering have been applied to the entire image sequence over a long observation period. For the slit scanning, however, no redundant data are acquired for tracking and position refinement. The depth has to be computed from the slit and a few additional pixels around it. We achieve this goal by using the stationary blur in the route panorama.

3. Stationary Blur in Route Panorama

3.1 Stationary Blur as Counterpart of Motion Blur

We find that distance features in the route panorama have blur along the t direction in the route panorama. This phenomenon is particularly obvious in the street scanning of urban areas. By examining the mechanism of this blur, we find it has similar characteristics as the motion blur but appears in the temporal domain. We name it *stationary blur* because it appears on points with low image velocities and, therefore, retaining at the slit position. The slower the camera velocity, the more the stationary blur is visible. If the camera stops, identical scenes are projected onto the slit so that horizontal patterns last along the time axis in the route panorama. This is similar as the motion blur stripes along the optical flow direction in the spatial domain, if the camera velocity is extremely fast.

It is well known that, under perspective projection, the image velocity is proportional to the camera translating speed and inversely proportional to the depth. For linear motion, stationary blur and motion blur appear in different ranges. If we illustrate the motion in EPI (Fig. 4a), the trace of a close feature may sweep across several (Δx) pixels in the image during the camera exposed time τ . The reflected light from the feature thus contributes to the intensities of multi-pixels in the image frame. Accordingly, the intensity collected at a pixel is the average from several neighboring points in the scene. The image intensity is obtained from the convolution between the surface color and a rectangular pulse. If the surface point is an edge, this average yields a motion blur [9]. A close feature with a high image velocity has severe motion blur [18]. On the contrary, a slow-moving point in the field of view retains at the same image position in several sampling instances (Δt), and is repeatedly captured by the slit (Fig. 4b). This causes the stationary blur along the t

axis in the route panorama. Distant objects appear to be stationary-blurred because of their slow image velocities.

Motion blur and stationary blur are not only related to depth. A convex path may produce more motion blur on objects over all ranges because of the additional rotation velocity, while a concave path may produce more stationary blur at objects close to the center of curvature of the path.

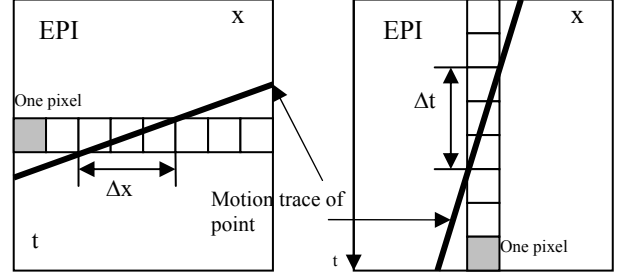


Fig. 4 Traces of fast and slow moving features in the EPI, which cause the motion blur in the image and stationary blur in the RP, respectively.

3.2 Formation of Stationary Blur in RP

Using the projection model discussed in Sec. 2, the slit width is ideally zero, the PoS is absolutely thin, and the sampling is infinitely dense on the camera path. In the real situation, the slit has a nonzero physical width and the route panorama is formed with narrow perspective projections (Fig. 5). Different depths, classified as *just-sampling* depth, *under-sampling* range and *overlapped-sampling* range, have different sampling characteristics. For scenes at the just-sampling depth, its views captured from consecutive slits can be connected without overlapping just as a normal perspective projection. At a depth closer than the just-sampling depth, consecutive slit views cannot cover a space completely and the scene is under-sampled. On the contrary, a point farther than the just-sampling depth may be covered by multiple slit views, which is an overlapped-sampling. The point color contributes to multiple slits over time, which is an aliasing in the time domain. If the point is an edge, its intensity change repeats along the time axis and results in a lower contrast in the route panorama than in the image.

We should not simply squeeze the route panorama along time axis to reduce the stationary blur on distance scenes, because this may deform a close scene at the same place. Although it has not been mentioned yet, the mosaicing doing local image deformation (expansion or squeezing) also has resolution changes similar as the stationary blur and the under-sampling.

The degree of the blur is related to depth Z , camera sampling rate m , path curvature κ , and vehicle speed V . If m and V are invariant locally over a linear path ($\kappa=0$), we can estimate the depth from the stationary blur.

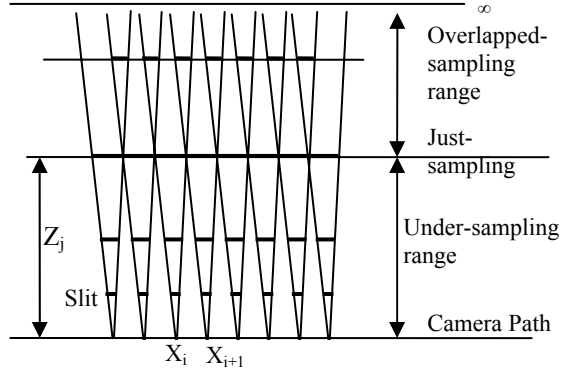


Fig. 5 Real projection of a route panorama (top view) by consecutive perspective cones distributed along the camera path.

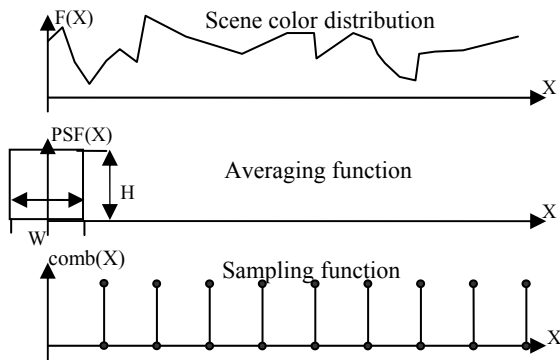


Fig. 6 Sampling route panorama.

In determining an intensity at a slit, colors of surface points covered by a Point Spread Function (*PSF*) are averaged. We approximate Gaussian *PSF* by a rectangle pulse with height H and span W normalized by $W \times H = 1$. The span W of the *PSF* at a certain depth Z is $W = 2Z \tan \theta$, where θ is half of the angle subtended by the cone. The averaging of scene color at Z corresponds to convolving color $F(X)$, which is unknown, with the pulse $PSF(X)$, i.e.,

$$I(X) = PSF(X) \otimes F(X) \quad (7)$$

where \otimes denotes the convolution. This phase is not different from normal perspective projection. In the sampling phase of the route panorama, the function

$$comb_p(X) = \sum_t \delta(X - t \times r) \quad (8)$$

with depth-independent interval r actually samples $I(X)$, where δ is the impulse function. The intensity $I(t)$ in the route panorama is finally obtained by

$$\begin{aligned} I(t) &= RP(X)|_{X=rt} = comb_p(X) \times PSF(X) \otimes F(X) \\ &= \sum_t \delta(X - t \times r) \int_{-w/2}^{w/2} F(X + s) PSF(s) ds \end{aligned} \quad (9)$$

for the symmetric *PSF*. As a comparison, sampling cones (*PSF*) of the perspective projection will not intersect each other, i.e., the sampling function at depth Z is

$$comb_l(X) = \sum_x \delta(X - xW) \quad (10)$$

and the image at the slit is

$$\begin{aligned} I(x) &= IM(X)|_{X=WX} = comb_l(X) \times PSF(X) \otimes F(X) \\ &= \sum_x \delta(X - xW) \int_{-w/2}^{w/2} F(X + s) PSF(s) ds \end{aligned} \quad (11)$$

From $I(t)$, we further approximate temporal differential $\partial I(t)/\partial t$ by temporal difference $\Delta_t I(t)$. Assume surface color $F(X)$ at depth Z has a discontinuity observable in the image (a large feature) as depicted in Fig. 7. The horizontal difference of the route panorama is

$$\begin{aligned} \Delta_t I(t) &= H \int_{-w/2}^{w/2} (F(s + (t+1)r) - F(s + (t-1)r)) ds \\ &= H \int_{-2/w}^{2/w} 2r \frac{\partial F}{\partial X} ds \end{aligned} \quad (12)$$

On the other hand, the spatial difference $\Delta_x I(x)$ at slit is

$$\begin{aligned} \Delta_x I(x) &= H \int_{-w/2}^{w/2} (F(s + (x+1)W) - F(s + (x-1)W)) ds \\ &= H \int_{-2/w}^{2/w} 2W \frac{\partial F}{\partial X} ds \end{aligned} \quad (13)$$

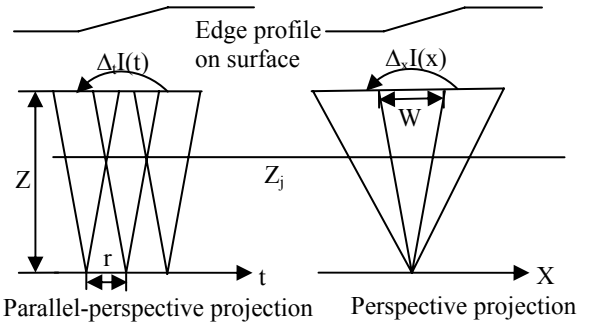


Fig. 7 PSF coverage of the route panorama and the image at the same position on a path.

4. Local and Global Estimations of Depth

4.1 Local Estimation Generating Dense Depth

We first examine the depth estimation from stationary blur at point level. Although the degree of stationary blur is related to the depth, the contrast distribution in the route panorama is insufficient to determine the depth independently because the original scene contrast distribution is unknown.

To obtain the spatial contrast at the slit, we calculate differential value in the images, as the route panorama is extended. $\partial I/\partial x$ is computable at l' if we wide the sampling slit to several neighboring pixels. We calculate $\partial I(t)/\partial t$ in the RP, and it reflects the contrast after

stationary blurring. The ratio of the spatial and temporal differentials provides the depth as (6), because

$$\frac{\partial t}{\partial x} = \frac{\partial I / \partial x}{\partial I / \partial t} \quad (14)$$

and thus the depth can be estimated by

$$Z(t) = -f \frac{V}{v} = -fV \left(\frac{\partial I / \partial x}{\partial I / \partial t} \right) \quad (15)$$

for a linear path. This is not used directly so far in the optical flow for the well-known reason that local optical flow can not generate accurate depth.

Here we examine the scope and resolution of the filtering for the local evaluation of ratio I_x and I_t . We use 3×5 Gaussian operators to calculate the spatial and temporal differentials $I_x(t,y)$ (which is $I_x(x,t,y)|_{x \in l}$). This reduces noise from the roughness of the route panorama.

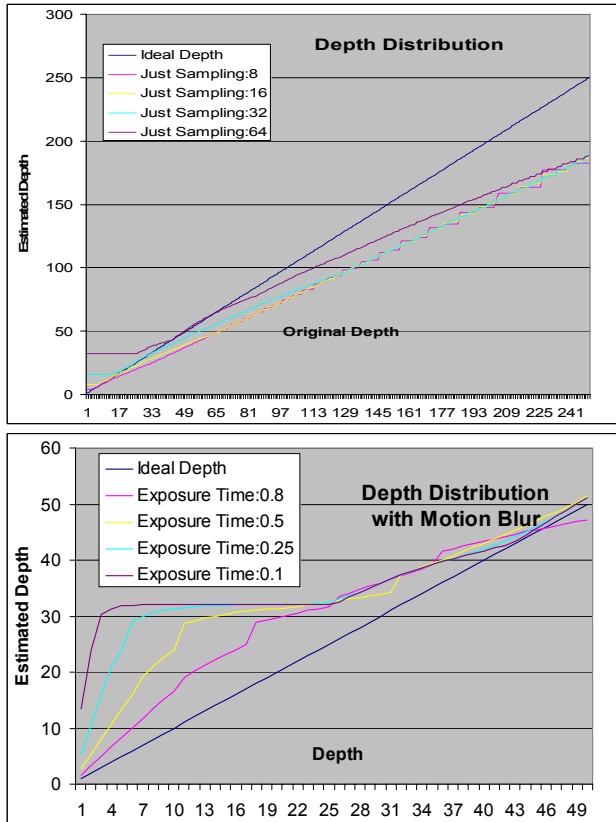


Fig. 8 Depth estimation on synthesized data. A step edge is put at all distances with 1m interval for measuring. (a) Different just-sampling depths are set to estimate the depths (colored curves). (b) Different exposure times are set to measure close depths. A longer exposure time produces a better depth at close range.

To test the algorithm, we locate an ideal step edge at all the depths and calculate its distribution by Eq. 15 for a set of just-sampling depths (Fig. 8). The results show that the

depth around the just-distance Z_j is better than depths of distance scenes and very close scenes. The error at an approximate range of $(2Z_j, \infty)$ is from the system when we choose a small operator scope Δt . Also, as the depth increases, the data level becomes coarse.

At the close range of $(0, Z_j/2)$, the measured depth is apparently more distant than its true value. This is caused by the under sampling effect where the location of the edge cannot be captured in consecutive slits completely, which is also possible to be interpreted by *Nyquist theorem*. Although reducing the just-sampling depth may improve the measure at close distances, the maximum frame rate and the resolution of the camera limits this possibility. On the other hand, if we extend exposure time of the frames (slow down shutter speed) to include the motion blur, the result is improved clearly in Fig. 8b. This is because the PSF sweeps a wider area over the sampling interval r , and the motion blur provides subtle changes in the slit views for the evaluation of spatial differential.

Using local data to yield depth instantly can avoid many complex issues such as occlusion, dynamic objects, and lack of feature in outdoor scene. In the real route panorama, other two feature selection criteria are added.

- The original level of feature contrast affects the resulting levels of I_x and I_t and then their ratio. We select reliable edges with high contrasts either in temporal or in spatial domain to calculate depth. A spatial-temporal gradient $g(t,y)$ not influenced by motion blur and stationary blur is calculated as

$$g(t,y) = \sqrt{(I_x(t,y))^2 + (I_t(t,y))^2} \quad (16)$$

for all y in the route panorama. Features satisfying $g(t,y) > \delta$ are selected for depth estimation.

- To avoid disturbance from features at different heights due to vehicle shaking and waving, we avoid near-horizontal features in the depth estimation by limiting edge orientations in the route panorama.

Figure 9 provides the result of the point-based depth measure, where spatial and temporal differential images are generated during input. The depths for the qualified points are computed. The ratio in (15) is displayed in gray levels. The brighter the point the closer the depth is, and vice versa. We can fill depth at empty points by using linear interpolation horizontally. This depth might be fine for visualization using layered representation, it is still very noisy and cannot yield satisfactory surfaces even we fit lines and planes over it. At the front lawn without many features, the depths are not reliable.

4.2 Depth from Global Measure of Blurs

The most significant result of the depth from stationary blur method is a global measure of the blurring. Instead of averaging or voting noisy data obtained from local depth

to obtain layered images, we use global measures of the spatial and temporal differentials separately and then estimate the reliable depth from their ratio.

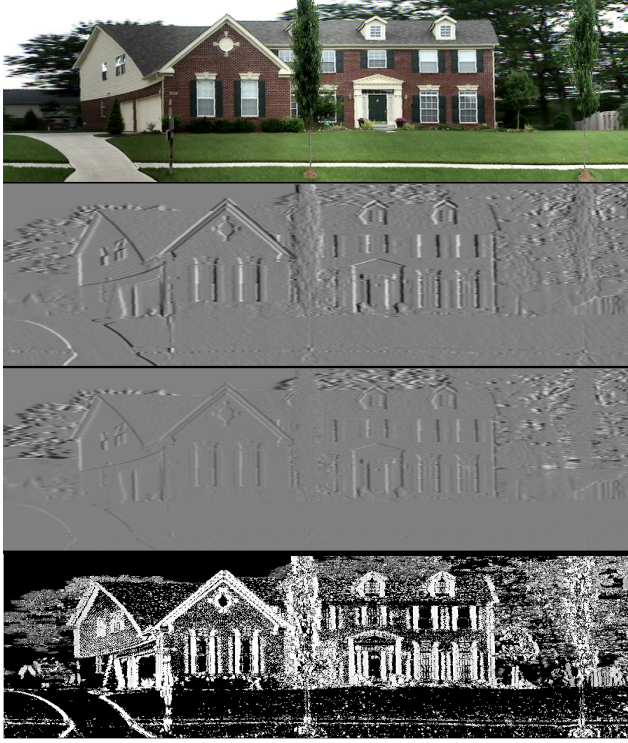


Fig. 9 A section of route panorama and its point based depth estimation. (a) RP (b) Temporal differential, (c) Spatial differential, (d) Estimated depth at points with high spatial-temporal gradient. The value of $\arctan(I_t/I_x)$ is displayed. Points without depth measure are set to zero.

Assuming an area σ in the route panorama captures an edge in the 3D space, we compute the averages of the spatial and temporal differentials respectively from all points with strong $g(t,y) > \delta$ in σ . According to (12) and (13), the ratio of the two averages is

$$\frac{\sum_{g(t,y) > \delta_1} I_x(t,y)}{\sum_{g(t,y) > \delta_1} I_t(t,y)} = \frac{\sum \Delta_x I(t)}{\sum \Delta_t I(t)} \quad (17)$$

$$= \sum 2 \int_{-w/2}^{w/2} \frac{\partial F}{\partial X} ds \bigg/ \sum H \int_{-w/2}^{w/2} 2r \frac{\partial F}{\partial X} ds = \frac{W}{r} = CZ$$

where C is a constant and the result is proportional to the depth. If an area is large to contain multiple features with positive and negative differential values, we calculate

$$\hat{Z} = \frac{\sum |\Delta_x I(t)|}{C \sum |\Delta_t I(t)|} \quad (18)$$

for the depth. This ratio of summarized differentials significantly reduces the noise and the result is more stable

than the average of depths from all points.

The average of the differentials can even be extended to irregular shapes after segmentation of the temporal route panorama, which has never been tackled in the optical flow computation. The resulting surfaces have more precise depths than layers (Fig. 11).

5. Experiments and Discussion

We have driven a vehicle through many streets to record complete route panoramas. For the route panorama shown in this paper, the vehicle speed is 20km/hr. A fixed sampling rate of the slit is set at 60HZ. On uneven roads, a vehicle suffers from additional shaking. Although the left-and-right translation will not happen, the vehicle roll (left-and-right swing) may have a big influence on the camera. Abrupt vertical translation due to the disturbance in vehicle pitch over a bumpy road will not be large and can be reduced by using a large vehicle with a long wheelbase and stable suspension. The video camera used has a shaking compensation function. A shaking removal algorithm has been developed to rectify the route panorama and then the corresponding differential images [19].

The motion blur may affect feature matching in the structure from motion. However, it does not influence the route panorama, because close objects with high image velocities leave their clear view in the RP. Our filtering method use $g(t,y)$ that is invariant to the motion blur in feature selection.

The entire scanning keeps the calculation of spatial differential within a very narrow stripe (5pixel for the operator size) around the slit; it is much less than image patches used for feature searching, matching, and stitching. The depth can be generated instantly because the algorithm uses a constant time for local computation and the complexity for the entire route panorama is linear ($O(S)$). The storage for the street model generation is only two imageries (RP and spatial differential images).

6. Conclusion

This work developed the stationary-blur based depth estimation for route panoramas. Through an elaborated analysis of blurs and motions, the proposed algorithm avoids feature matching and tracking in structure from motion methods. It can generate robust depth measure efficiently without being influenced by occlusion, motion blur, and other complex situations. From the data storage perspective, the spatial differential and the route panorama stored are much less than EPIs used in tracking, and image patches used for stitching. It keeps the data compactness for sensor and system development. Moreover, the

continuous and non-redundant route panorama greatly simplifies the model generation. It will broaden applications of slit scanning to real time visual archiving of cityscapes for communication and visualization.

References

- [1] J. Y. Zheng, S. Tsuji, Panoramic representation for route recognition by a mobile robot. *Int. Journal on Computer Vision*, 9(1), 55-76, 1992.
- [2] J. Y. Zheng, S. Tsuji, Generating dynamic projection images for scene representation and understanding. *Journal of Computer Vision Image Understanding*, 72, (3), 237-256, Dec. 1998.
- [3] D. G. Aliaga, I. Carlbom, Plenoptic stitching: a scalable method for reconstructing 3D interactive walkthroughs, *SIGGRAPH01*, 2001.
- [4] Z. Zhu, A. R. Hanson, E. M. Riseman, Generalized parallel-perspective stereo mosaics from airborne video. *IEEE Trans. PAMI*, 26(2), 226-237, 2004.
- [5] J. Y. Zheng, M. Shi, Mapping cityscapes to cyber space, *Int. Conf. CyberWorld 2003*, pp. 166-173, 2003.
- [6] J. Y. Zheng, Digital route panorama, *IEEE Multimedia*, 10(3), 57-68, 2003.
- [7] T. Kawanishi, K. Yamazawa, H. Iwasa, H. Takemura, N. Yokoya, Generation of high-resolution stereo panoramic images by omnidirectional imaging sensor using hexagonal pyramidal mirrors, *14th ICPR*, Vol. 1, pp. 485-489, 1998.
- [8] S. Li, A. Hayashi, Robot navigation in outdoor environments by using GPS information and panoramic views, *Proc. IEEE/RSJ Int. Conf. on Intelligent Robots and Systems*, pp. 570-575, 1998.
- [9] M. Ben-Ezra, S. K. Nayar, Motion deblurring using hybrid imaging, *CVPR03*, 657-665, 2003.
- [10] D. Zomet, D. Feldman, S. Peleg, D. Weinshall, Mosaicing new views: the crossed-slits projection, *IEEE Trans. PAMI*, pp. 741-754, 2003.
- [11] H. Baker, R. Bolles, Generalizing epipolar-plane image analysis on the spatial-temporal surface, *Proc. CVPR-88* pp.2-9.
- [12] C-K. Tang, H-Y. Shum, Efficient dense depth estimation from dense multi-perspective panoramas, *ICCV 2001*.
- [13] Z. Zhu, A. R. Hanson, 3D LAMP: a new layered panoramic representation, 2, 723-730, *ICCV 2001*.
- [14] H. Zhao, R. Shibasaki, A Vehicle-borne urban 3D acquisition system using single-row laser range scanners, *IEEE Trans. on SMC, B*: 33(4), 2003.
- [15] S. Srinivasan, Extracting structure from optical flow using the fast error search technique, *IJCV*, Vol. 37, 203-230, 2000.
- [16] J. Weng, Y. Cui, N. Abuja, Transitory image sequences, asymptotic properties, and estimation of motion and structure, *IEEE Trans. PAMI*, 19(5), 451-464, 1997.
- [17] A Wang, E. H. Adelson, Representing moving images with layers. *IEEE Trans. Image Processing*, 3(5):625-638, 1994.
- [18] J. S. Fox, Range from translational motion blurring, *IEEE CVPR88*, pp. 360-365, 1988.
- [19] J. Y. Zheng, Stabilizing route panorama, *17th ICPR*, 348-351, 2004.

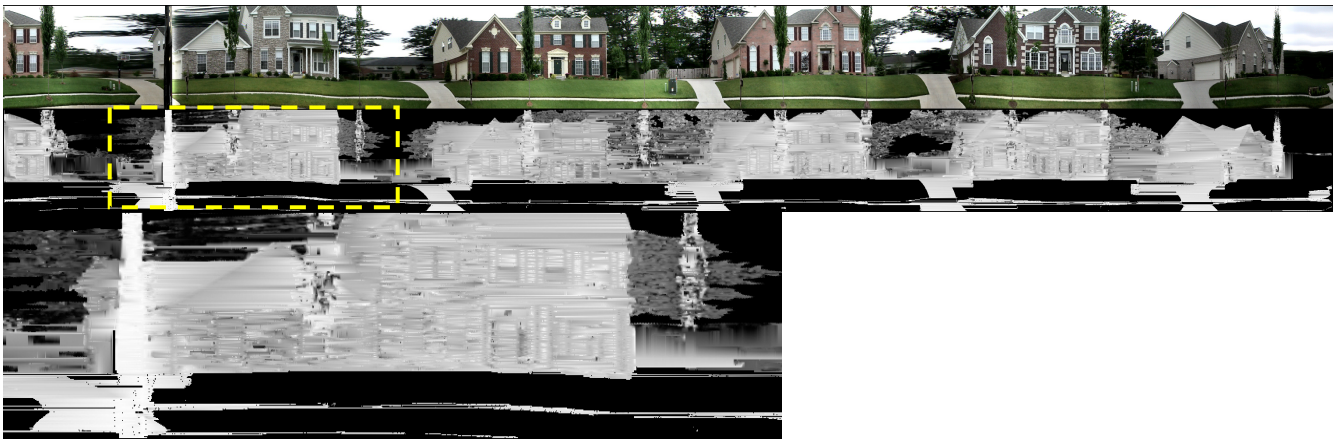


Fig. 10 Route Panorama and estimated depth mpa. (a) route panorama, (b) depth map after filling empty holes with neighboring measured points, (c) an enlarged section of depth map.



Fig. 11 Surface model of a street from global patches after segmentation.